WEMo (Wave Exposure Model): Formulation, Procedures and Validation

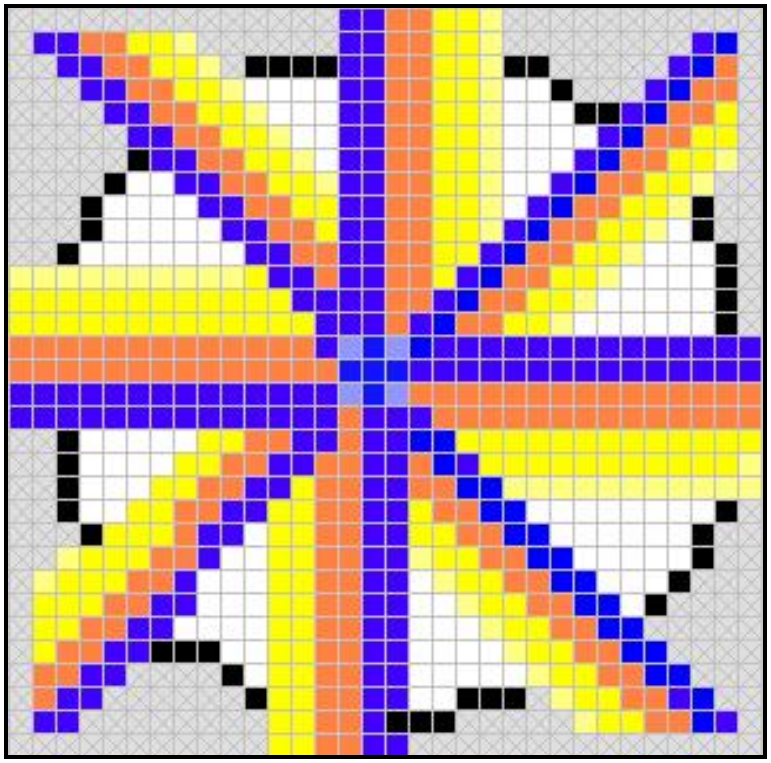

NOAA Technical Memorandum NOS NCCOS #65

This report has been reviewed by the National Ocean Service of the National Oceanic and Atmospheric Administration (NOAA) and approved for publication. Mention of trade names or commercial products does not constitute endorsement or recommendation for their use by the United States government.

Citation for this Report

Malhotra, A., and M. S. Fonseca. 2007. WEMo (Wave Exposure Model): Formulation, Procedures and Validation. NOAA Technical Memorandum NOS NCCOS #65. 28p.

WEMo (Wave Exposure Model): Formulation, Procedures and Validation

Amit Malhotra
Mark S. Fonseca

Center for Coastal Fisheries and Habitat Research at Beaufort
NOAA/NOS/NCCOS
101 Pivers Island Road
Beaufort, North Carolina 28516

NOAA Technical Memorandum NOS NCCOS #65

October 2007

United States Department of Commerce
Carlos M. Gutierrez
Secretary

National Oceanic and Atmospheric Administration
Conrad C. Lautenbacher, Jr.
Administrator

National Ocean Service
John (Jack) H. Dunnigan
Assistant Administrator

CONTENTS

FIGURES

TABLES

Abstract. This report describes the working of National Centers for Coastal Ocean Service (NCCOS) **W**ave **E**xposure **Mo**del (**WEMo**) capable of predicting the exposure of a site in estuarine and closed water to local wind generated waves. WEMo works in two different modes: the Representative Wave Energy (RWE) mode calculates the exposure using physical parameters like wave energy and wave height, while the Relative Exposure Index (REI) empirically calculates exposure as a unitless index. Detailed working of the model in both modes and their procedures are described along with a few sample runs. WEMo model output in RWE mode (wave height and wave energy) is compared against data collected from wave sensors near Harkers Island, North Carolina for validation purposes. Computed results agreed well with the wave sensors data indicating that WEMo can be an effective tool in predicting local wave energy in closed estuarine environments.

KEYWORDS: WEMo, wave exposure, wind wave exposure, wave energy, wave height, relative exposure index, REI, representative wave energy, RWE, fetch.

1. INTRODUCTION

Coastal managers and ecologists are often confronted with tasks to estimate wave parameters in coastal and estuarine environments since hydrodynamic factors can profoundly impact the environment in coastal areas. This involves estimating the wave energy reaching the shoreline taking into account the effects of wind, local topography and bathymetry. WEMo was designed to bridge the gap between ecologists and managers on one hand, and physical hydrologists on the other by providing a user-friendly access to quantitative forecasts of wave energy in estuarine environments. In this report we describe the National Centers for Coastal Ocean Service (NCCOS) Wave Exposure Model (WEMo) to perform such computations. It describes the formulation of WEMo in both Representative Wave Energy (RWE) and Relative Exposure Index (REI) modes and validation of RWE mode (wave height) against the observational data collected near Harkers Island, North Carolina.

2. WEMo

WEMo is a simple hydrodynamic model that calculates the wind wave exposure of a site (Murphey and Fonseca 1995, Fonseca and Bell 1998). WEMo's two distinct modes-- Representative Wave Energy or RWE mode and Relative wave Exposure Index or REI mode-- use different approaches to calculate wind wave exposure. RWE mode is based on linear wave theory and is implemented with a wave ray technique in a monochromatic approach. REI mode on the other hand uses an empirical approach based on inverse-distance-weighting function (IDW) of bottom depth applied to wave rays. IDW function represents that bottom depth variations close to a site have more effects on the exposure values than far away depth variations (Murphey and Fonseca 1995). Selection of WEMo mode depends on the project requirement, geographical area for the study and time scale used in the study.

2.1 Formulation of RWE Mode

WEMo's Representative Wave Energy or RWE mode carries out computations as a numerical one-dimensional model. RWE values computed by WEMo are based on linear wave theory and ray tracing technique making it a model of Lagrangian nature in a sense that the wave generation and dissipation is considered while traveling with the waves along rays. RWE represents the total wave energy in one wave length per unit wave crest width. RWE units are J/m or $kg/m/s^2$ (USCOE 1977).

WEMo computes the wave height for RWE mode in a monochromatic approach, i.e., along each fetch ray generated by winds in the same direction. Waves generated are propagated along the fetch rays. Propagating water waves over irregular bottom bathymetry involves dissipation processes like shoaling, refraction, diffraction and energy dissipation. In order to decrease complexity and computation time, dissipation due to refraction and diffraction of the waves are neglected and dissipation is carried out by shoaling, wave breaking and bottom friction over downwind distance over water. Refraction of waves in monochromatic, unidirectional wave-ray approach results in unrealistic results, especially

behind shoals and islands (Holthuijsen et al. 1989). The final output for RWE mode is the combined effect of wave generation, propagation and dissipation over weighted fetch to account for shoreline irregularities.

Fetch

Growth and dissipation of wave energy are highly sensitive to the wave direction; thus, it is required to consider each narrow band of directions. In restricted fetch areas i.e. coastal plains and closed estuaries, there is no one dominant wind or wave direction. Measuring fetch at various angles around a site approximates the relative exposure of that site to waves approaching from different directions (Puotinen 2005). WEMo calculates the fetch for all the directions to simulate the wave exposure in an estuarine and closed environment.

Figure 1a shows the rays (10 km) generated for a site each at $\pi/16$ angular resolution. Ray distance is adjustable in WEMo though 10 km is the default.

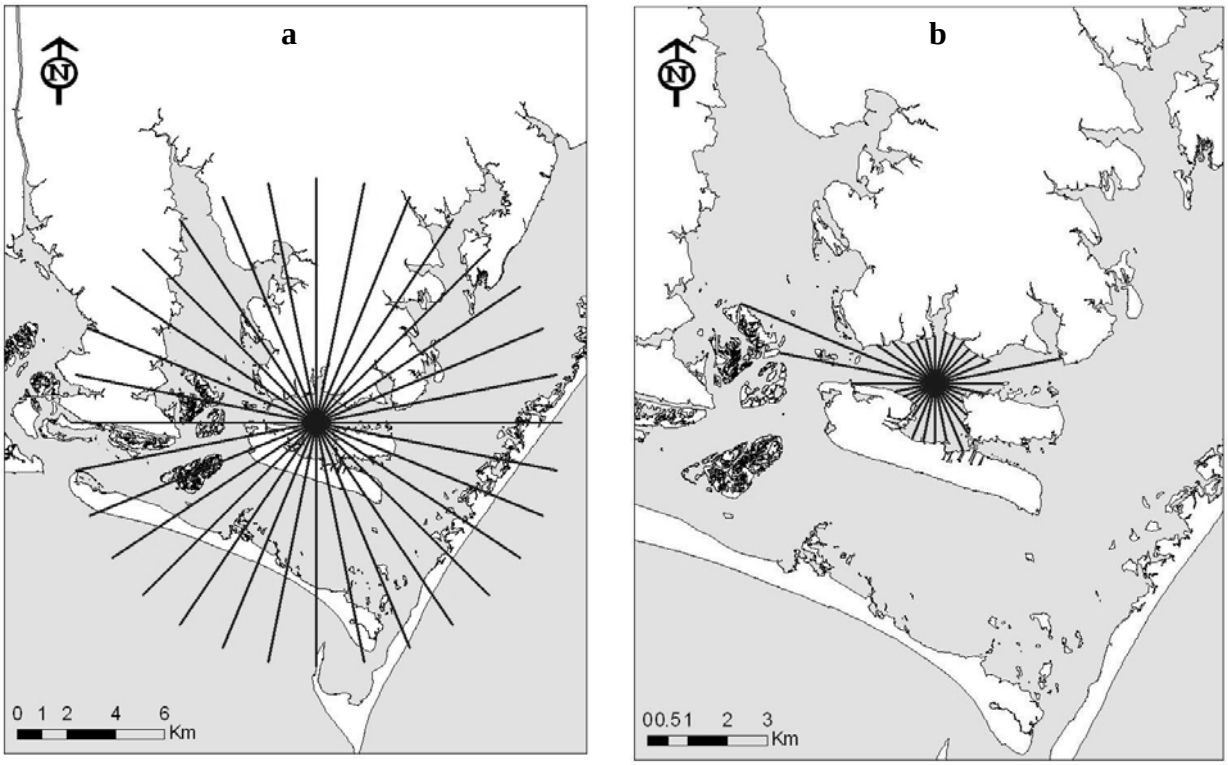

Figure 1a. 10km rays generated for a site at 11.25^{o} angular resolution. Figure 1b. Fetch rays for that site.

The fetch is defined as the uninterrupted distance from the site to land along a given compass heading. Figure 1b shows the fetch rays for the site.
Due to irregular shoreline in coastal waters the simple fetch length in a given compass direction is not very effective since the width of fetch places a substantial restriction on the fetch length (USCOE 1977). Therefore, the fetch is modified by taking the cosine weighted average of all the rays within a certain sector on either side of the fetch ray defined by

angle φ. The cosine weighted fetch is named as effective fetch and is defined by Eq. 1 or Eq. 2.

$$Eff\ F_i = \frac{\int_{-\varphi}^{+\varphi} F_j \cos(\theta)\, d\theta}{\int_{-\varphi}^{+\varphi} \cos(\theta)\, d\theta} \quad (1)$$

where,

$Eff\ F_i$= Effective fetch for the ith direction fetch ray

F_j = length for j radiating fetch ray after clipping to shoreline and interrogating bathymetry

or,

$$Eff\ F_i = \left(\sum_{j=-n}^{n} F_j \cos(\theta_j) \right) \Big/ \left(\sum_{j=-n}^{n} \cos(\theta_j) \right) \quad (2)$$

θ_j = angle between the ith fetch ray and the jth ray

n = number of rays selected by user ranging from 2 for 16 rays to 8 for 56 rays

Effective fetch in WEMo is calculated by summing the product of fetch length and cosine of the angle of departure from the ith heading over each of *n* number of fetch rays and dividing by the sum of the cosine of all angles (Eq. 2). Figure 2a and 2b show the fetch rays and effective fetch rays, respectively. Effective fetch rays look trimmed down in the figure compared to fetch rays. This method is based on assumption that wind moving over water surface transfers energy to the water in the direction of the wind and in all directions within $\pi/4$ radians (45^o) on either side of the wind direction. (USCOE 1977)

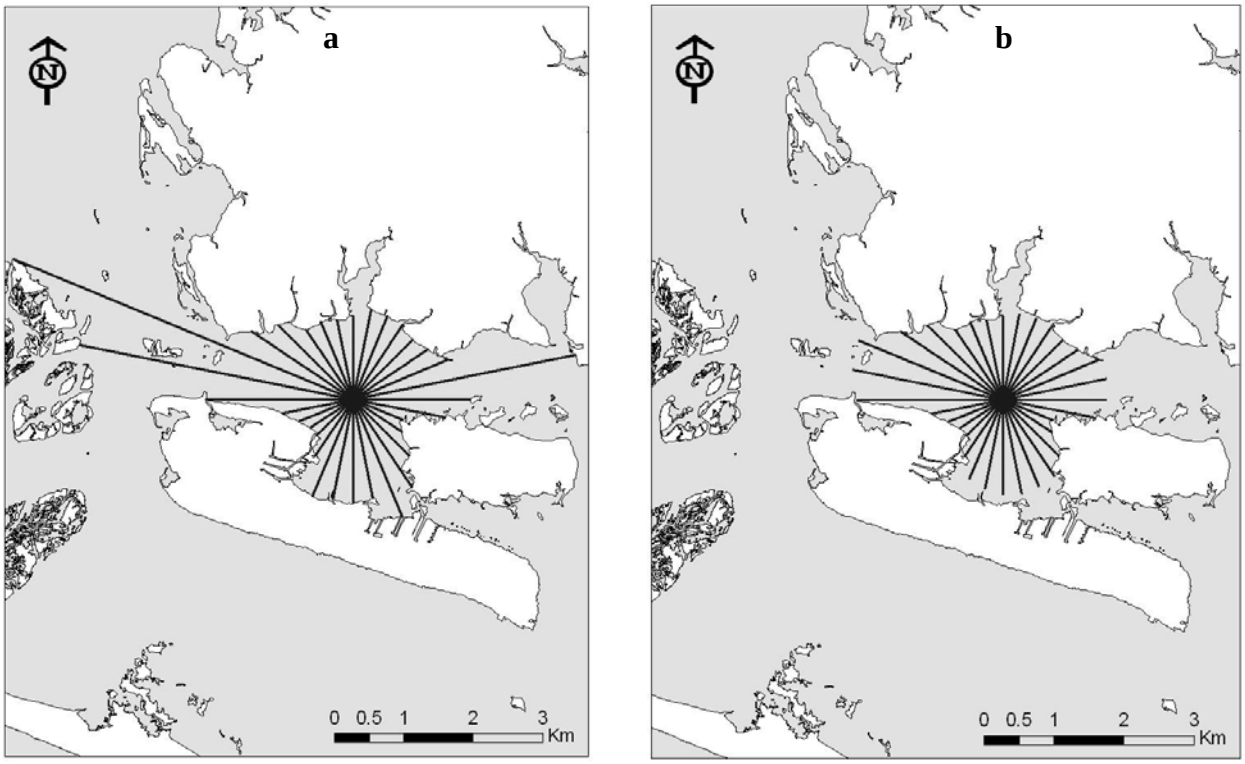

Figure 2a. Fetch rays for a site. Figure 2b. Effective fetch rays for that site. Note: Big fetch rays are trimmed down due to effect of fetch width.

In WEMo the number of rays included in the effective fetch calculation depends on the angular resolution or number of rays selected by the user. WEMo has the option to select total number of rays in ranges between 16 and 56 (Figures 1 and 2 show 32 rays). Uncomplicated, linear shorelines can probably be accurately assessed using the lower number of rays while highly crenulated shorelines with complicated intervening bathymetry should use the maximum number of rays.

Wind Input

Each effective fetch ray has an associated wind speed and wind frequency. These wind parameters are calculated from the hourly wind data obtained from various agencies or in situ data collected by the user. WEMo calculates the wind speed and corresponding frequency for every 6.43^{o} (56 rays) angular resolution and is resampled or linearly interpolated for any other angular resolution. Wind frequency for a direction is defined as the ratio of number of hours wind blow from that direction and the total number of hours of wind data as shown in Eq. 3.

$$\omega_j = \frac{number\ of\ hour\ wind\ blow\ in\ direction\ j}{Total\ number\ of\ hour\ of\ wind\ data} \tag{3}$$

WEMo also provides the option of selecting the subset of the wind dataset based on the wind speed. Subset option helps to select the data causing the most damage to shoreline and habitat.

Wave Height

Waves propagate along each of the effective fetch rays based on the wind speed in the same direction and the underlying depth around the area. The wave reaching the site goes through a series of wave propagation and wave dissipation steps. Eq. 4 forms the basis of the model.

$$H = H_W - (H_{s+B+f}) \quad (4)$$

where,

H is the wave height reaching the site, H_W is the wave height generated by the wind alone and H_{s+B+f} describes the rest of the external physical phenomena contributing to the wave height. They can be either positive [shoaling (s)] or negative [shoaling, wave breaking (B) and bottom friction (f)].

Wave propagation and generation highly depend on the depth of water in which they propagate. According to linear (Airy) wave theory, waves are classified into categories based on the water depth. Three general categories are defined in the Table 1 according to the magnitude of d/L where d is the water depth and L is the wavelength.

Table 1: The classification of waves based on ratio of water depth (d) and wave length (L) according to linear wave theory

Classification	d/L
Deep	>1/2
Intermediate	1/25 to 1/2
Shallow	< 1/25

For shallow and intermediate water, wind waves are propagated based on the Sverdrup-Munk-Bretschneider (SMB) method revised by Bretschneider (Bretschneider 1967, Hasselmann et al. 1975). Significant wave height is predicted using Eq. 4 or using SMB curve in Figure 3

$$H_w = 0.283 \tanh\left[0.530\left(\frac{gd}{U^2}\right)^{0.75}\right] \tanh\left\{\frac{0.0125\left(\frac{gF}{U^2}\right)^{0.42}}{\tanh\left[0.530\left(\frac{gd}{U^2}\right)^{0.75}\right]}\right\}\frac{U^2}{g} \qquad (5)$$

where,
U = wind speed,
H_w = significant wave height,
F = fetch length,
g = acceleration due to gravity,
d = average depth along the fetch.

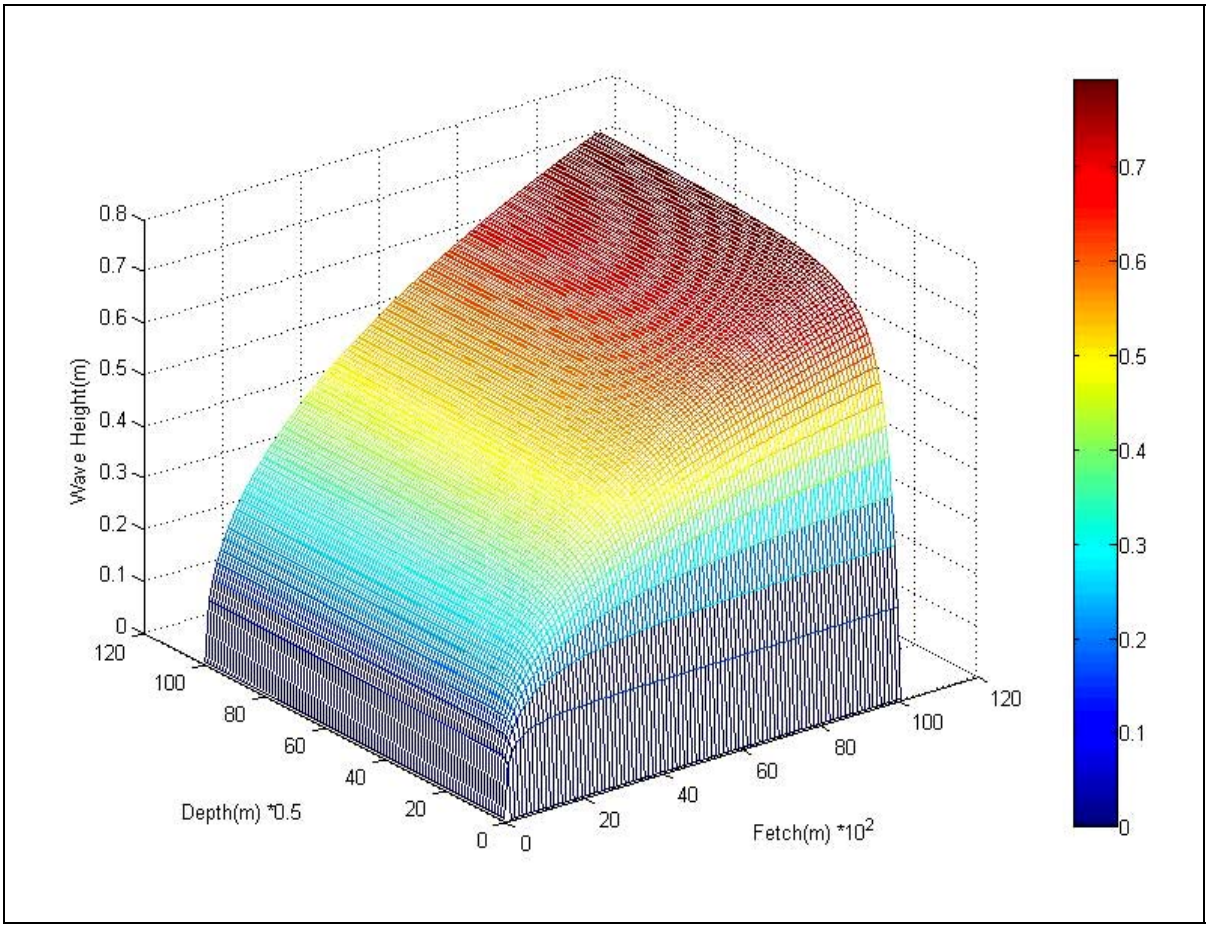

Figure 3. SMB curves for shallow water: Wave Height vs water depth and effective fetch at constant wind speed of 12m/s.

For deep water as d/L → 0.5, the equation simplifies to

$$H_w = 0.283 \tanh\left[0.0125\left(\frac{gF}{U^2}\right)^{0.42}\right]\frac{U^2}{g} \qquad (6)$$

Figure 4 shows the SMB curves for the deep water in the range of 0 to 20 m/s winds and 0 to 10 km fetch.

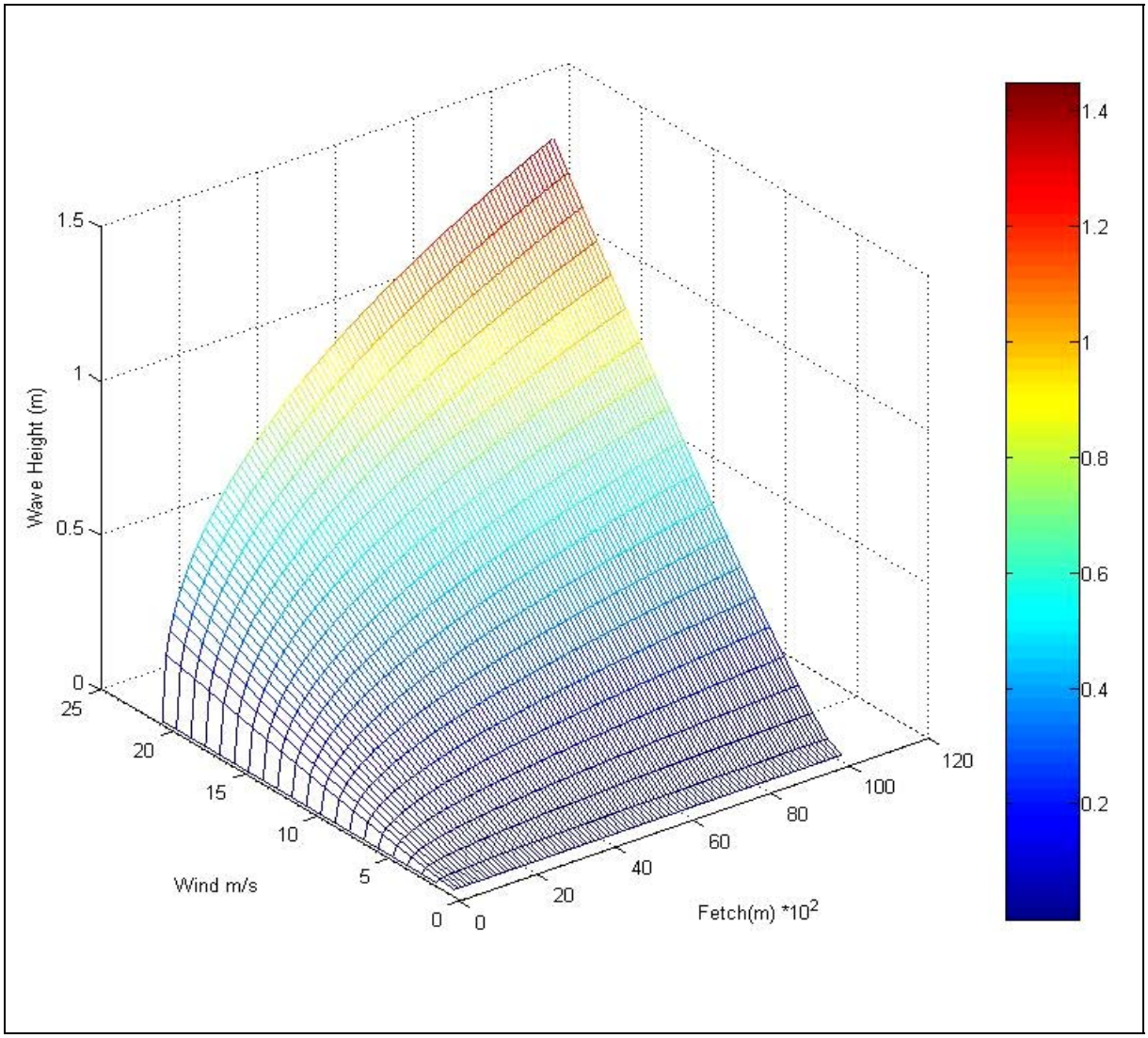

Figure 4. SMB curves for deep water: Wave Height vs wind speed (0 – 20m/s) and effective fetch.

For shallow and intermediate waters Eq. 5 predicts significant wave height only for average depth; to overcome this limitation each effective fetch ray is divided into small segments and Eq. 4 is applied to the quantized segments. Figure 5 shows an example of main segmentation of an effective fetch ray, divided primarily into two main segments.

Both fetch segments are further divided into smaller segments though at different resolutions controlled by the bathymetry selected for the run and the user input. In the example in Figure 5, fetch segment 1 is divided at a finer resolution compared to fetch segment 2 because being closer to the site any changes in bathymetry around segment 1 will have higher effect on the generated wave. To get the maximum results, fetch segment 1 is divided into segments equals to the resolution of bathymetry used for the run. Resolution for the division of fetch segment 2 is set by the user in the model depending on the underlying bathymetry.

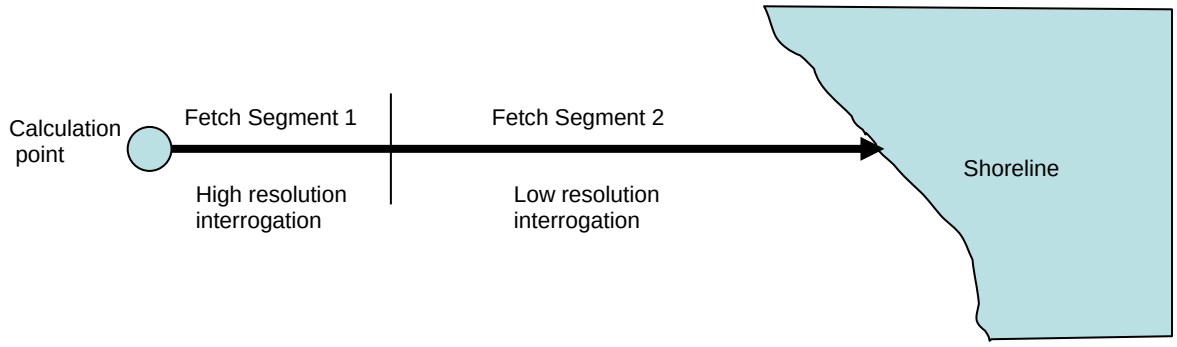

Figure 5: Example of segmented effective fetch ray, divided primarily into two main segments, Fetch segment 1 and Fetch segment 2.

For term H_{s+B+f} (Eq. 4), each contributing phenomena for wave height is calculated separately. Like the wave generation term H_w, this computation starts from the shoreline side of the fetch segment 2 successively. At each individual segment, the model checks and accounts for wave shoaling and wave breaking. Wave speed and wave length decrease in shallow water thereby increasing the wave height since energy per unit area increases. When wave height becomes too steep, it become unstable and breaks (Dean and Dalrymple 1991). Wave height after shoaling effect is calculated iteratively by solving Eq. 7 and 8.

$$H_s = H_o \left[\frac{k}{k_o} \left(\frac{1}{1 + \frac{2kd}{\sinh 2kd}} \right) \right]^{1/2} \tag{7}$$

As per the dispersion equation in linear wave theory (Dean and Dalrymple 1991)

$$k_o = \sigma^2 / g \ = k d \tanh k d \tag{8}$$

where,

H_s = wave height after shoaling effect,

H_o = wave height in deep water,
k = wave number,
σ =
d = water depth,
g = acceleration due to gravity.

According to Eq. 7 as $d/L_o > 0.05$, H_s / H_o is less than 1 for intermediate water and it gets equal to 1 for deeper water. On the other side as $d/L_o < 0.05$, waves start experiencing nonlinear behavior and occurrence of wave breaking (Dean and Dalrymple 1991).

In deep water, wave breaking limit is generally set at $H_o/ L_o = 1/7$, but this is not appropriate for shallow water (Dean and Dalrymple 1991). Wave breaking limit in shallow water depends not only on the relative depth H/L ratio but also on the beach slope (Sorensen 1993). The expression for wave breaking implemented in the model for shallow water is (Goda 1985, Wood et al. 2001)

$$\frac{H_b}{L_0} = A\left[1-\exp\left(-1.5\frac{\pi d_b}{L_0}\left(1+15\tan^{4/3}\alpha\right)\right)\right] \tag{9}$$

where,
H_b = wave height at breaking,
L_0 = wave length in deep water,
A = 0.17 (default) Goda coefficient (Goda 1985)
d_b = water depth at breaking,
$\tan\alpha$ = 1/30 (default) beach slope

There are different phenomena for dissipation of wave energy at the sea bottom: dissipation due to bottom friction, viscous boundary flow and percolation. Bottom friction is the most prominent among all (Carniello et al. 2005). Hence bottom friction is the only one considered in the model. Below is the expression for estimating friction decay factor (Putnam and Johnson 1949, Bretschneider and Reid 1954).

$$K_f = \left[1+\frac{64\pi^3}{3g^2}\frac{f\,H_1\,\Delta x}{T^4}\frac{K_s^2}{\sinh^3\left(2\pi d/L\right)}\right] \tag{10}$$

where,
K_f = friction decay factor,
f = friction factor,
T = wave period,
K_s = shoaling coefficient,

Δx = segment of fetch length.

When depth-induced wave breaking is present, effects of bottom friction are comparatively negligible and only wave breaking is considered in the model.

Final wave energy calculation is done using Eq. 11 as a final output after computing wave height and wave period for each of the effective fetch rays.

$$RWE = C \sum_{i=1}^{n} \left(H_i^{\,2} \; T_i^{\,2} \tanh\left(k_i \, d_i\right)\right)\omega_i \qquad (11)$$

where,
C = constant,
H_i = wave height in ith effective fetch ray direction,
T_i = wave period in ith effective fetch ray direction,
k_i = wave number,
d_i = depth,
ω_i = wind frequency in ith effective fetch ray direction (Eq. 3)

The final outputs of WEMo's RWE mode is representative wave energy (RWE), maximum wave height (MaxWvH), maximum wave direction (MaxWvD) and average wave height (AvgWvH) for each site.

Assumptions made in formulation of the RWE WEMo model are:

- Linear harmonic propagating waves for an incompressible fluid
- No surface tension
- Water depth changes slowly compared to wave length
- No wave reflection due to change in water depth
- No refraction and diffraction considered
- Sea is assumed at full arisen state a condition where waves are in equilibrium with the wind; hence no wind duration is considered
- Locally generated wind waves are prominent source of waves and no ocean swells are considered

2.2 Formulation of REI mode

The second mode of WEMo empirically calculates a Relative wave Exposure Index (REI) as the combined effect of wind, fetch and bottom depth. WEMo REI mode does not compute the wave energy, as in WEMo RWE mode, but a unitless index. No work has been done to compare REI values with wave energy values, though REI is a good indicator for comparing among sites under similar conditions and close geographic extent (e.g., the same estuary).

REI is computed with hourly wind speed and direction, fetch and bathymetry data. REI of a site is calculated using Eq. 12. (Murphey and Fonseca 1995, Fonseca and Bell 1998)

$$\text{REI} = \left(\sum_{i=1}^{8} EffF_i \; V_i \; D_i \} \right) / 8 \qquad (12)$$

where

$EffF_i$ = Effective fetch for the ith direction

V_i = Wind speed for the ith direction

D_i = Wind duration for the ith direction

Similar to RWE mode, the fetch is calculated by creating rays from the site and clipping them to the nearest shoreline. In REI mode, the region is divided into eight compass directions of 45^o sectors and hourly wind speeds are obtained for these 8 sectors. Eight zones are further divided to account for the fetch width, making total of 32 rays (not changeable) at increment of 11.25 ^{o} (Keddy 1982). By weighting these multiple fetch measures for each compass heading, termed as effective fetch $EffF$, we account for irregularities in shoreline geometry that could misrepresent the potential of wind wave development from a given compass heading (USCOE 1977). Effective fetch for each compass direction is calculated using Eq. 13.

$$EffF_i = \left(\sum_{j=0}^{4} f_j \cos(\pi/16\, j) + \sum_{j=5}^{8} f_j \cos(\pi/16\,(j-4)) \right) \Bigg/ \left(\sum_{j=0}^{4} \cos(\pi/16\, j) + \sum_{j=5}^{8} \cos(\pi/16\,(j-4)) \right) \qquad (13)$$

$EffF_i$ = Effective fetch for the ith direction

f_j = length for j radiating ray after clipping to shoreline and interrogating bathymetry

To calculate f_j, 32 rays are radiated from the site at 11.25 ^{o} increments in all directions. The maximum length of each ray is fixed at 10 km (adjustable in WEMo) as this distance was considered to be sufficient to generate a maximum wave height effect for coastal systems following empirical experimentation with the USACOE Automated Coastal Engineering System software version 1.07 (USCOE 2007). These rays are clipped with the region's shoreline to get the exact fetch in that particular direction; Figure 6a

shows an example of unclipped fetch rays and Figure 6b shows that fetch rays clipped to the shoreline.

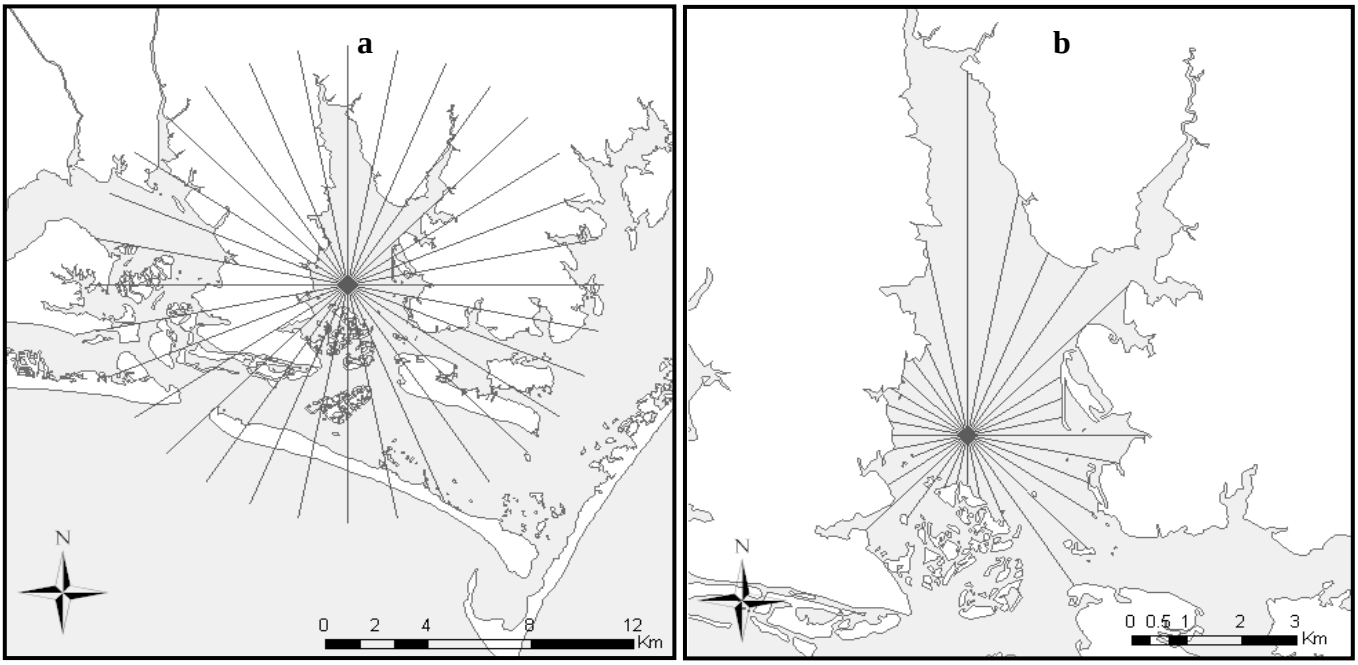

Figure 6a. Lines represent the unclipped fetch rays for 32 directions for a site in North River, NC. Figure 6b. Shows fetch rays clipped to the shoreline.

Depth variations in the area drastically influence the wind waves generated. These effects of bathymetry are included in WEMo and are controlled by an inverse distance power function (Eq. 14 and 15) i.e., shallow water near a given point has a greater effect on damping exposure than shallow water at a greater distance.

$$f_i = \int_0^L \frac{(1 - x/L_i)}{(x)^{p_w}} z_x \, dx \qquad (14) \qquad \text{or} \qquad f_i = \int_0^L PF \; z_x \, dx \qquad (15)$$

where,

f_j = length for j radiating ray after clipping to shoreline and interrogating bathymetry,

x = distance from the site along the clipped ray,

L_i = total length of the ith clipped ray,

Z_x = depth at the distance x along the clipped ray,

p_w = power of the function depending on the wind speed at the site,

0 – 13.41 (m/s)	p_w = 0.053
13.41 – 26.82 (m/s)	p_w = 0.062
> 26.82 (m/s)	p_w = 0.082

PF = power function governing the fetch.

WEMo interrogates the bathymetry grid at a fixed distance for each clipped ray since bathymetry data input for WEMo is in raster format. Therefore, Eq. 14 and 15 transform to Eq. 16 and 17, correspondingly. This fixed distance could be decided based on the underlying bathymetry for the area of interest, but generally kept less than the bathymetry grid resolution to capture all the information in the grid.

$$f_i = \sum_{j=0}^{L/n} \left[1/(D_j)^{p_w} \ (1 - D_j / L_i) \right] Z_j \qquad (16)$$

or $$f_i = \sum_{j=0}^{L/n} PF \ Z_j \qquad (17)$$

where,

f_j = length for j radiating ray after clipping to shoreline and interrogating bathymetry,

D_j = jth interrogating distance from the site along the clipped ray,

L_i = length of the ith clipped ray,

Z_j = depth at the distance D_j along the ith clipped ray,

n = fixed distance for bathymetry interrogating,

p_w = power of the function depending on the wind speed at the site,

0 – 13.41 (m/s)	p_w = 0.053
13.41+/ – 26.82 (m/s)	p_w = 0.062
> 26.82 (m/s)	p_w = 0.082,

PF = power function governing the fetch.

The power p_w of the power function PF (Eq. 15 and 17) depends on the wind speed at the site and accounts for the mitigating effect of depth on the REI as the fetch increases. The Army Corps of Engineers Shore Protection Manual (USCOE 1977) was used as a reference to derive powers of the power function. SPM includes wave height versus fetch graphs which are used for verification purposes. Wave height graphs were plotted against the fetch for two depths (1.5 m and 3.05 m) that are typical depths for submerged aquatic vegetation in our study sites and depths where shallow water waves of the size found in estuaries frequently interacts with the seafloor. Wind speed positively influences wave height generation with increasing fetch. Wave height was normalized to the maximum height attained by a wave for a particular wind speed and depth. After normalization of the curves, a power function was fit to wave height development curves for wind speeds of 6.7, 8.94, 11.18, 13.41, 17.88, 22.35, 26.82, 31.29, 35.76 and 44.7 m/s (15, 20, 25, 30, 40, 50, 60, 70, 80 and 100 mph), at both the depths. For ease of application, we collapsed these curves into three arbitrary categories (0-13.41 m.s^{-1}, 13.41 +/– 26.82 m/s and > 26.82 m/s) and each category was assigned a power function derived by averaging the powers from the curves for each category (0.053, 0.062 and 0.082, respectively); Figure 7 shows the graph of power function PF plotted against the fetch values from 0 to 10 km range.

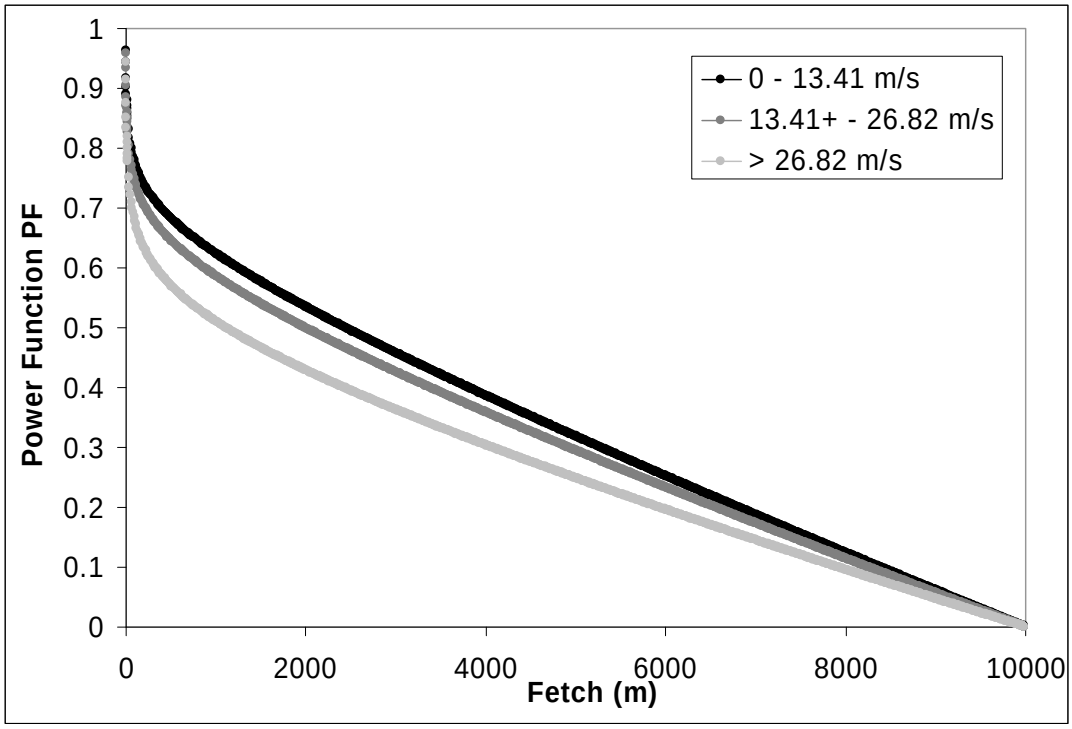

Figure 7. Graph showing a plot between Fetch and Power Function PF for three wind categories

These curves were converted into cumulative curves to emulate the SPM curves derived above. After assigning power for each wind category, each ray generated from the site in the eight compass sectors will have a power for the power function. However, the four rays radiating out from either side of the i^{th} compass heading at increments of 11.25 degrees will not have any wind speed associated, and hence lacks a power for the function. To assign a power for intermediate rays, a linearized average function was used between adjacent i^{th} compass headings to calculate intermediate powers. For example, if easting has power of 0.082 and northing has power of 0.062 then,

1^{st} intermediate rays power –> 0.082 + (0.062 – 0.082)/4 = 0.077

2^{nd} intermediate rays power –> 0.082 + 2*(0.062 – 0.082)/4 = 0.072

3^{rd} intermediate rays power –> 0.082 + 3*(0.062 – 0.082)/4 = 0.067.

As suggested by p_w values, as wind speed increases the effect of bathymetry along the rays on REI index decreases, which is generally true as higher winds push bigger waves over the bathymetry.

3. VALIDATION

To assess the behavior of the RWE mode of WEMo, the model predictions were compared against the observations from the wave sensors installed in the field. Validation of WEMo in REI mode was not carried out since there was no easy way of comparing field collected data with REI values.

3.1 Wind and wave data

A wave sensor was deployed at Dredge Island near Harkers Island, North Carolina (Figure 8) in two sessions lasting around 3 weeks each. These sites were chosen due to easy access and the contrasting conditions among the two sites, where the north site is exposed to long fetches from the Core Sound; whereas, south side is protected from north fetch behind the Dredge Island.

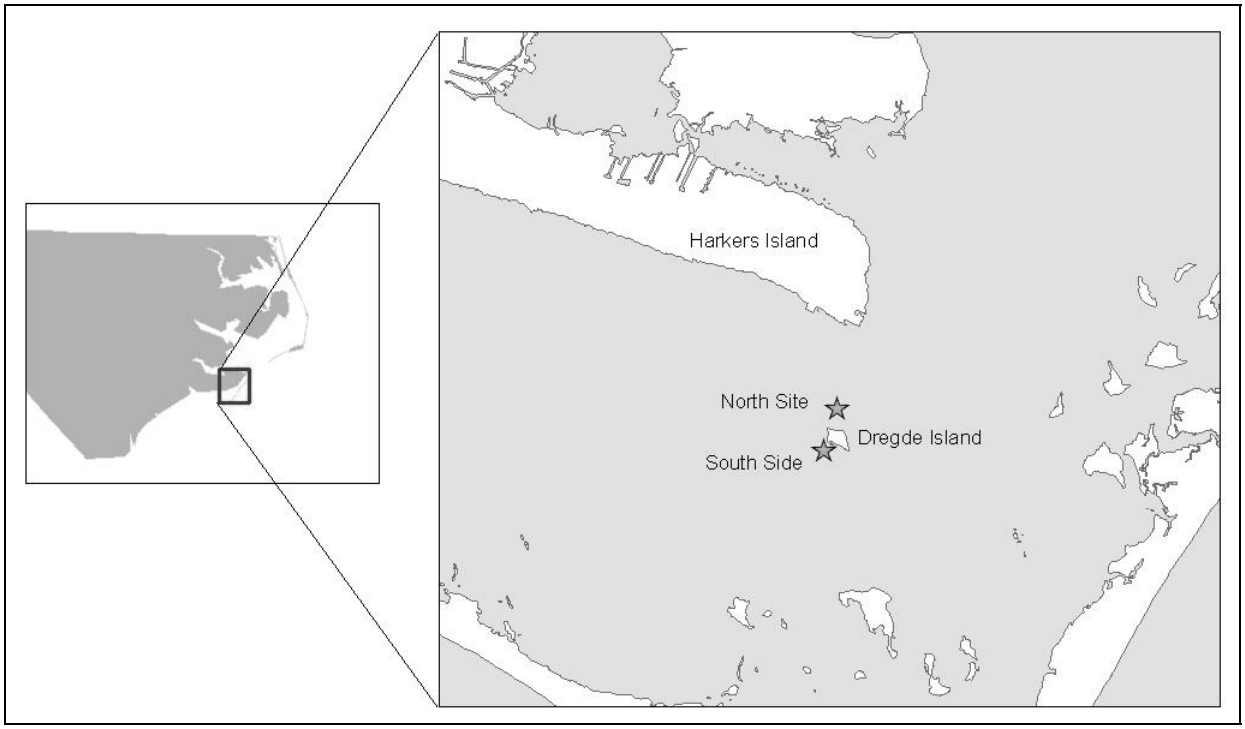

Figure 8. Sensor locations for session 1 at North Site and session 2 at South Site

RBR wave and tide sensor 'TWR 2050' was mounted on the piling at the north site (34^{o} 40' 37" N, 76 ^{o} 31' 43 W) for session 1 lasting from December 15, 2006, to January 7, 2007, and subsequently at the south site (34^{o} 40' 25" N, 76 ^{o} 31' 47" W) for session 2 lasting from January 12, 2007, to January 30, 2007. At both sites the sensor was set to record bursts of pressure data every 30 min at a sampling rate of 4Hz for 128 s. Sensor was installed at 1 m above the bottom for both the sessions to reduce the effect of depth of wave attenuation and also to keep it submerged during low tides. Bathymetry at both sites is shallow ranging from a 1 m to maximum of 5 m. Boating activity was minimal during those time periods around the area. Wave height and wave period data were derived from the pressure and depth data recorded by the sensor using Fast Fourier Transformation (FFT) analysis for each burst period. The barometric pressure sensor was installed outside at Pivers Island, North Carolina and its data were utilized to correct the underwater pressure data.

National Data Buoy Center NDBC's C-MAN Station at Cape Lookout, North Carolina (NDBC 2007) supplied wind data for the two sessions. Cape Lookout, North Carolina located at 34°37' 18" N, 76 ° 31' 30" W with an anemometer height of 14.4 m above sea level. The wind data obtained were in hourly increments with wind speed (m/s) and wind direction (degrees from true north). Wind speed data is plotted in Figure 9a and 9b for session 1 and session 2. The time series of the wind data for session 1 (Figure 9a) shows a wind event occurred during December 26 – 27, 2006.

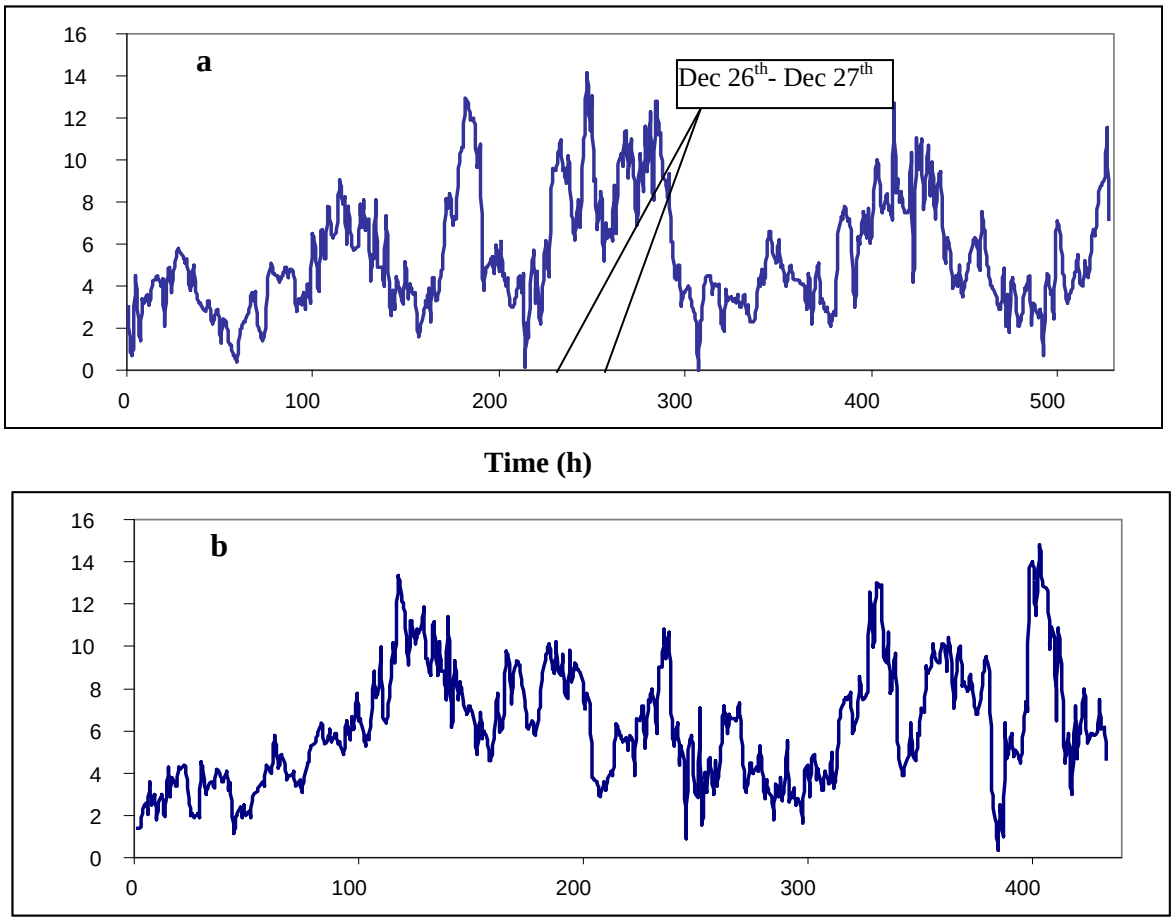

Figure 9a. Time series plot of wind speed (m/s) for session 1 starting from Dec 15th 2006 12:00 h up to Jan 7th 2007 12:00 h. Figure 9b. Time series plot of wind speed for session 2 starting from Jan 12th 2007 12:00 h up to Jan 30th 2007 12:00 h.

3.2 Processing

Wave sensor and wind data from NDBC were at two different temporal resolutions; to get both data sets on same time scale wave data were averaged every hour. Maximum wave height observed for the session 1 at north site was 0.52 m and for session 2 at south site was 0.40 m. To remove the randomness and variability from the observed wave data set and provide enough wind data to run the model, moving average analysis was employed. Figure 10a and 10b shows the observed wave height plots for session 1 and 2

respectively after applying the 6 hour moving average. Time series of wave and wind data were strongly correlated, since in closed estuaries like coastal North Carolina locally generated winds mostly dominate the wave generation and not the ocean swells (Weiqi et al. 2002). The effect of ocean swells is mostly limited to the mouth of bays or inlets.

To obtain model predicted data for the same period for session 1 and session 2, WEMo RWE was set to run using bathymetry and shoreline data obtained from Coastal Survey Development Lab (CSDL) NOAA and National Ocean Service (NOS) NOAA vector shoreline dataset, respectively. The bathymetry data was resampled at 20 m resolution and converted to MLLW from NAVD 88 using NOS VDatum (Hess et al. 2005). Wind data was processed into WEMo RWE format using 6 hours of data with steps of 1 hour to simulate the 6 hour moving average analysis done on observed wave data. WEMo was put to run in batch processing mode for 528 wind files for session 1 and 440 wind files for session 2.

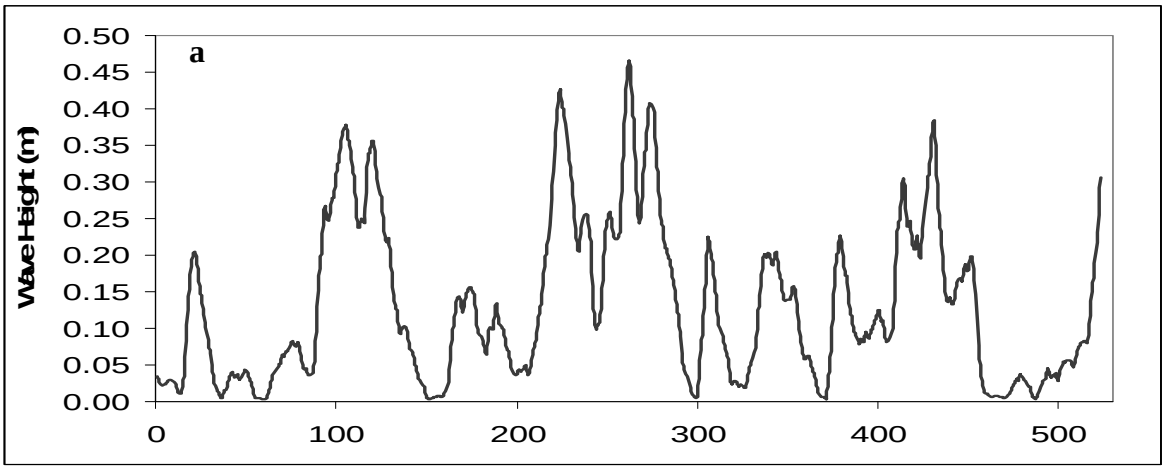

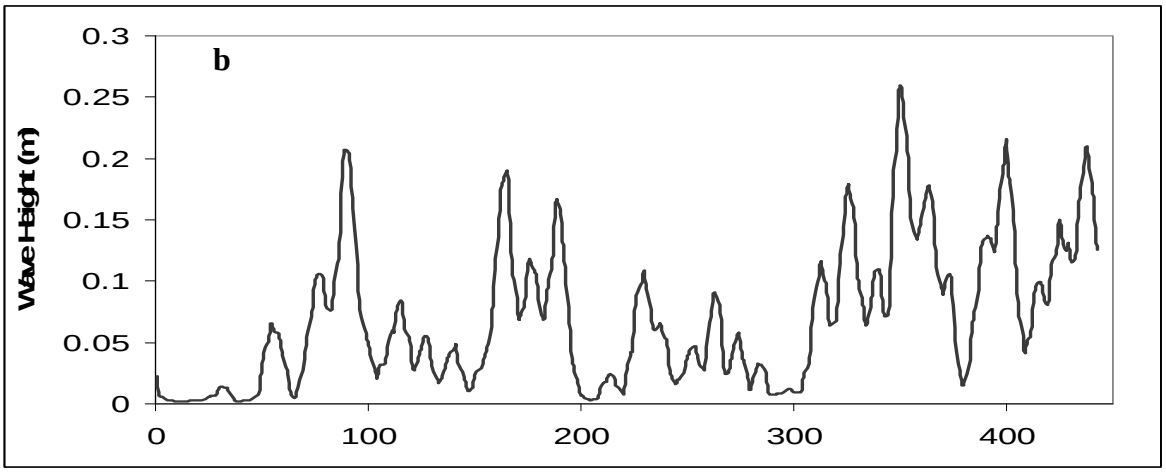

Figure 10a. Time series plot of wave height for session 1 starting from Dec 15th 2006 12:00 hrs up to Jan 7th 2007 12:00 hrs. Figure 10b. Time series plot of wave height for session 2 starting from Jan 12th 2007 12:00 hrs up to Jan 30th 2007 12:00 hrs.

3.3 Data analysis and comparison

This section discusses the comparison between the model results and the observed data and discusses statistical results. Figure 11 shows the time series plot of observed wave height data (sensor) and predicted wave height data (WEMo) for session 1 and session 2. Significant wave height predictions from WEMo relates to the observed values quite well for both the sessions. The response of the model looks good as wind velocity changes are well predicted by the model and prediction follows the trend of observed waves.

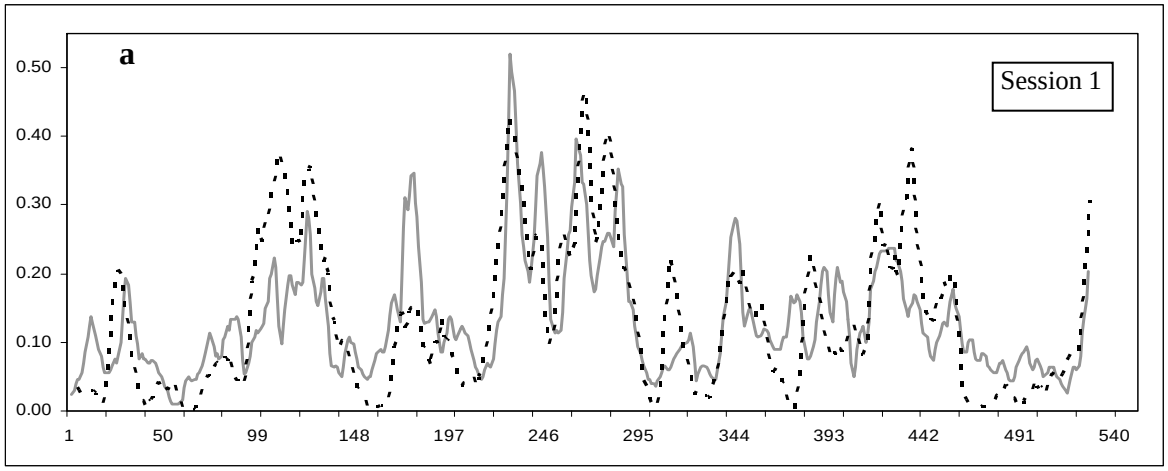

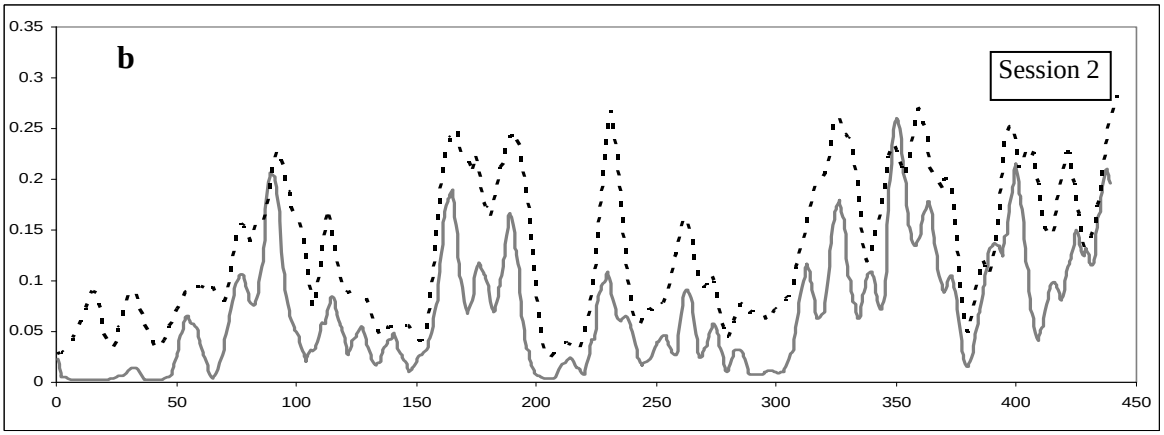

Figure 11a. Time series plot comparing observed sensor wave height (m) (solid line) and WEMo model predicted wave height (m) (dashed line) for session 1 starting from Dec 15th 2006 12:00 hrs up to Jan 7th 2007 12:00 hrs. Figure 11b. Time series plot comparing observed sensor wave height (solid line) and WEMo model predicted wave height (dashed line) for session 2 starting from Jan 12th 2007 12:00 hrs up to Jan 30th 2007 12:00 hrs. Note: Y axis is wave height in meter.

Time series visual comparison shows that overall model prediction is slightly higher than the observed predictions, more so in case of session 2. This over-prediction could be due to

the presence of seagrass beds in the surrounding areas of the south site that reduces the wave height not accounted in the model. Friction caused by submerged vegetation like seagrass bed was not considered in the model. This could be applied to sensor 1 location also for limited cases, depending on the direction from where wind blows. Session 1 has few time periods where sensor wave heights are higher than predicted wave height. Detailed wind direction analysis was not conducted to quantify this difference but the over-prediction in session 2 could be explained by wave refraction at the southern site as waves approaching from the north will focus and defocus around the shoals of Dredge Island. Another reason for over prediction could be that no modification to wind data was conducted for anemometer height since it was higher than the normal standard height of 10 m above mean sea level.

Visual inspection of time series also shows lag in response time between observed and predicted wave height. Response time lag could be explained due to the distance between wind station and wave sites and time period it take to start creating the wind waves. The lag seems to be varying depending on the changing direction of the wind. Overall time series analysis predicts a good behavior of the model compared to the observed data. This analysis is good for observing and checking the response part of the model, statistical tests will further explain the overall model performance.

Figure 12a-b shows the scatter plot of observed wave heights Vs predicted wave heights for session 1 and 2 respectively. In each plot the linear regression line shows the trend in comparison to the ideal model line. For both sessions at low wind speeds model tends to predict slightly higher than the observed data. The coefficient of determination (R-squared) calculated for the linear regression for session 1 was $R_1^2 = 0.62$ and session 2 $R_2^2 = 0.69$. Also the intercept of regression line in both session are similar suggesting the bias caused by WEMo's over-prediction at low wind speeds. For session 2 regression line seems to be parallel to the ideal line suggesting that over-prediction is consistent for the range of the plot.

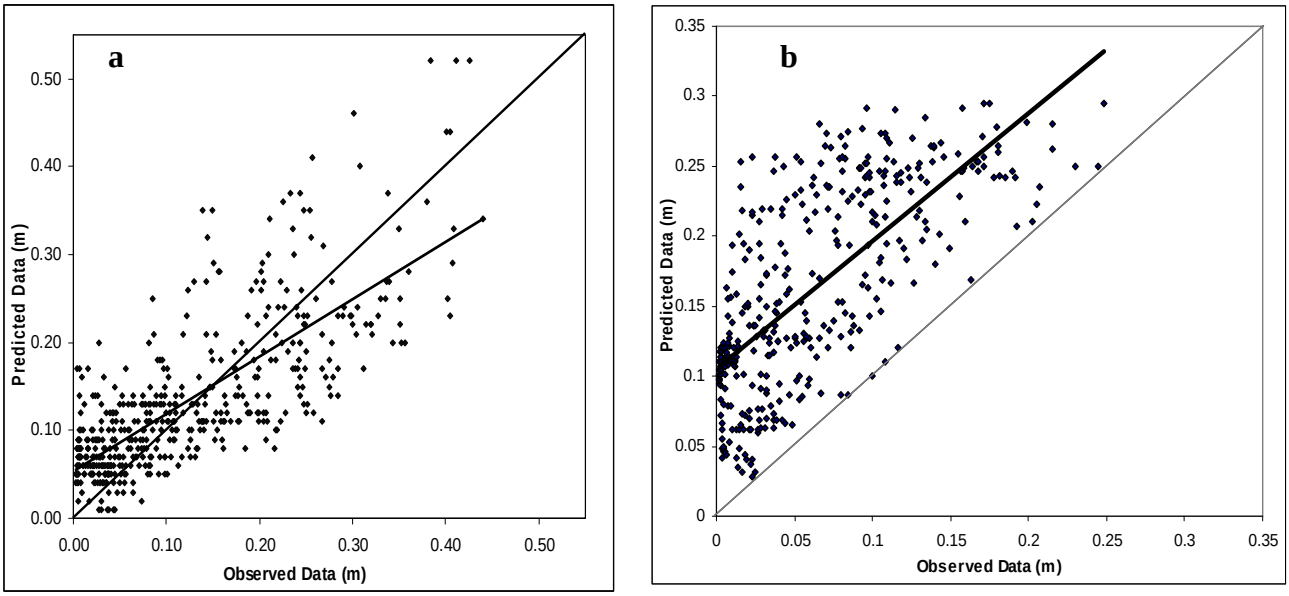

Figure 12a-b. Scatter plot of observed sensor wave height and WEMo model predicted wave height for session 1 and session 2. Light line = ideal fit, Dark line = regression generated from the data.

For further statistical comparison of observed and model predicted wave height, data from both the sessions were combined (Weiqi et al. 2002). Data points with low wave height were not appropriate for the analysis due to the high variability in sensor data. Therefore, wave height data lower than 1 cm was removed from the analysis. The sample size of the data after combining two data sets and removing the inappropriate data was N = 814. Using the combined data set RMS error for wave height was 6 cm. The bias predicted by the model at 6 cm indicates that WEMo over predicted the significant wave height (where mean observed value is 0.16 cm). Over-prediction bias is mostly due to the over predicted wave heights by WEMo for low wind speeds. Since mean value of the observed data set is low it adds to the over predicted bias.

To determine the performance of the model in comparison to the ideal model, a suitable measure was defined, called performance rate (Holthuijsen et al., 1989).

$$Performance\,rate \;=\; \frac{RMS\,(error)}{RMS\,(observed\,change)} \qquad (18)$$

Using Eq. 18, performance rate calculated for the combined data set was 0.54 as unity is for the perfect model. To check the bias in the dataset, scatter index (SI) was calculated. Scatter index is defined as the RMS error normalized by the mean observed value of the reference quantity (Weiqi et al, 2002)

$$SI \;=\; \frac{RMS\,(error)}{mean\,observed\,value} \qquad (19)$$

Scatter index calculated using Eq. 19 was 0.38 indicating that RMS error is 38% of the mean observed value. Again low mean for observed value i.e. low wave heights observed for majority of the time period added to the scatter index. Selecting a subset of dataset would have reduced the SI further.

4. CONCLUSIONS

Wave Exposure Model (WEMo) is a simple hydrodynamic model for predicting the wind wave exposure of a site by either utilizing the wave height and derived wave energy calculated using one dimensional wave-ray model of RWE mode or by using an empirical approach of REI mode.

RWE mode validation compared model predictions against in situ wave data collected from two sites in southern Core Sound in Eastern North Carolina. This area is dominated by locally generated fetch limited wind seas. Significant wave heights observed were highly correlated with the wind data obtained from C-Man station.

WEMo shows a good response in predicting the changes in the wave height as wind changes velocity. Wave height predictions are slightly higher than the observed wave heights due to the use of universal friction factor (sand) in the model and not accounting for friction due to underlying habitat. Another reason for over prediction could be that no modification to wind data was conducted though anemometer was higher than the normal standard height of 10 m above mean sea level. Response time lag observed by visual inspection could be explained due to the separation-distance between wind station and wave sensor sites and time period it take to create the wind waves. The varying lag depends on the direction of the wind. Future work for validation involves the installation of directional wave sensors and its comparison to the model predictions in both high and low wave environments.

Overall significant wave heights predicted by the RWE mode agreed well with observed data and provide a viable option to compute wave exposure for a site. Ease-of-use, easily available input data and low CPU and memory requirement make WEMo a fairly useful tool for ecologists, coastal and resource managers and others looking for simple way to predict wave height and energy. Further testing is required in varied geographical areas and more test sites to make it a widely accepted tool.

5. ACKNOWLEDGEMENTS

Development of this model has been supported by intramural funding of Applied Ecological Research and Restoration (AERR) branch at Center for Coastal Fisheries and Habitat Research, NOS, NOAA. Authors would like to express their appreciation to Erik D. Davenport, Gregory A. Piniak and Patti M. Marraro CCFHR who reviewed the report and provided excellent comments.

6. REFERENCES

Bretschneider, C. L. 1967. Fundamentals of Ocean Engineering – Part 1. Ocean Industry, 2: 56-108.

Bretschneider, C. L., and R. O. Reid. 1954. Modification of Wave Height Due to Bottom Friction, Percolation, and Refraction. U.S. Army Corps of Engineers, Beach Erosion Board, Washington D.C.

Carniello, L., A. Defina, S. Fagherazzi and L. D'Alpaos. 2005. A Combined Wind Wave-Tidal Model for the Venice Lagoon, Italy. Journal of Geophysical Research, 110 (F04007): 1-15.

Dean, R. G. and R. A. Dalrymple. 1991. Water wave mechanics for engineers and scientists**.** World Scientific Publishing, Singapore.

Fonseca, M. S., and S. S. Bell. 1998. Influence of physical setting on seagrass landscapes near Beaufort, North Carolina, USA. Marine Ecology Progress Series. 171: 109-121.

Goda, Y. 1985. Random Seas and Design of Maritime Structures. University of Tokyo Press, Tokyo, Japan. 75-82.

Hasselmann, K., D. B. Ross, P. Muller, and W. Sell. 1975. A parametric wave prediction model. Journal of Physical Oceanography 6: 200-228.

Hess, K. W., E. Spargo, A. Wong, S. A. White, and S. K. Gill. 2005. VDatum for Coastal North Carolina: Tidal Datums, Marine Grids, and Sea Surface Topography. NOAA Technical Report NOS CS 21. U.S. Department of Commerce, National Oceanic and Atmospheric Administration, Silver Spring, Maryland. 46p.

Holthuijsen, L. H., N. Booij and T. H. C. Herbers. 1989. A prediction model for stationary, short crested wave in shallow water with ambient currents. Coastal Engineering 13: 23-54.

Keddy, P. A. 1982. Quantifying within-lake gradients of wave energy: interrelationships of wave energy, substrate particle size and shoreline plants in Axe Lake, Ontario. Aquatic Botany 14: 41-58.

Murphey, P. L., and M. S. Fonseca. 1995. Role of high and low energy seagrass beds as nursery areas for *Penaeus duorarum* in North Carolina. Marine Ecology Progress Series 121: 91-98.

National Data Buoy Center (NDBC). 2007. NGDC/WDC MGG, Boulder-Geophysical Data System GEODAS. Internet file: http://www.ngdc.noaa.gov/mgg/geodas/geodas.html. Last accessed 8/22/2007.

Puotinen, M. L. 2005. An automated GIS method for modeling relative wave exposure within complex reef-island systems: a case study of the Great Barrier Reef, 1437-1443. In: Zerger, A. and Argent, R. (Eds.) MODSIM 2005. International Congress on Modelling and Simulation. Modelling and Simulation Society of Australia and New Zealand, Melbourne, Australia.

Putnam, J. A., and J. W. Johnson. 1949. The Dissipation of Wave Energy by Bottom Friction. Transactions of the American Geophysical Union 30: 67-74.

Sorensen, R. M., 1993. Basic Wave Mechanics For Coastal and Ocean Engineers. John Wiley & Sons, New York.

U.S. Army Corps of Engineers, Coastal and Hydraulics Laboratory. 2007. Automated Coastal Engineering System software (ACES). Internet file: http://chl.erdc.usace.army.mil/chl.aspx?p=s&a=ARTICLES!455. Last accessed 8/22/2007.

U.S. Coastal Engineering Research Center (USCOE). 1977. Shore Protection Manual, Vol. 1. U.S. Army Coastal Engineering Research Center, Ft. Belvoir, Virginia.

Weiqi, L., L. P. Sanford, and S. E. Suttles. 2002. Wave measurement and modeling in Chesapeake Bay. Continental Shelf Research 22: 1048-1061.

Wood, J. D., M. Muttray, and H. Oumeraci. 2001. The SWAN model used to study wave evolution in a flume. Ocean Engineering 28: 805-823.

United States Department of Commerce

Carlos M. Gutierrez
Secretary

National Oceanic and Atmospheric Administration

Vice Admiral Conrad C. Lautenbacher, Jr. USN (Ret.)
Under Secretary of Commerce for Oceans and Atmospheres

National Ocean Service

Jack Dunnigan
Assistant Administrator